Magnetic fluctuations and superconducting pairing in ϵ-iron

A. S. Belozerov[1,2], A. A. Katanin[3,1], V. Yu. Irkhin[1,2] and V. I. Anisimov[1,2]

[1]*M. N. Miheev Institute of Metal Physics, Russian Academy of Sciences, 620108 Yekaterinburg, Russia*
[2]*Ural Federal University, 620002 Yekaterinburg, Russia*
[3]*Moscow Institute of Physics and Technology, 141701 Dolgoprudny, Russia*

We study Coulomb correlation effects and their role in superconductivity of ε-iron under pressure from 12 to 33 GPa by using a combination of density functional and dynamical mean-field theory. Our results indicate a persistence of the Fermi-liquid behavior below the temperature $\sim$1000 K. The Coulomb correlations are found to substantially renormalize the density of states, reducing the distance from the peak to the Fermi level to 0.4 eV compared to 0.75 eV obtained in DFT calculations. We find significant antiferromagnetic correlations, which are accompanied by the formation of short-lived local magnetic moments. We use the obtained results as a starting point for construction of the multiband Bethe-Salpeter equation, which eigenvalues indicate that antiferromagnetic spin fluctuations may result in the superconducting pairing in ε-Fe. Moreover, the tendency to superconducting instability becomes weaker with the increase of pressure, which may explain the disappearance of superconductivity at $\sim$30 GPa.

I. INTRODUCTION

Since the discovery of the hexagonal close-packed (hcp) iron (ε phase) in 1964 [1], its puzzling properties have attracted significant interest. This phase appears at pressures above 12 GPa and, as shown by static compression experiments, is stable up to pressures and temperatures corresponding to Earth's core conditions [2]. It makes the investigation of ε-Fe is particularly relevant for geophysics and Earth's magnetism [3,4].

One of the actively debated characteristics of ε-Fe is its magnetic behavior. The Mössbauer effect measurements found no hyperfine magnetic field at temperatures down to 30 mK [5–8], implying that hcp iron is nonmagnetic. The static magnetic order was not also detected by x-ray magnetic circular dichroism (XMCD) [9] and neutron powder diffraction [10]. The anomalous mode splitting in the Raman spectra [11], interpreted initially as a hint of the presence of magnetic order, was later shown to be inconsistent with it [12]. At the same time, the x-ray emission spectroscopy (XES) consistently detected remnant magnetism, decreasing with pressure up to $\sim$35 GPa [10,13,14].

The presence of magnetic correlations in ε-Fe is supported by density functional theory (DFT) studies. Most of early calculations predicted the antiferromagnetic type-II (AFM-II) ground state, which is stable up to $\sim$50 GPa [15–18], or the spin-spiral ground state [19,20]. It is worth noting that AFM-II structure leads to a better agreement of structural and elastic properties with experiments, as compared to nonmagnetic calculations [15,16]. Nevertheless, recent DFT study of Lebert *et al.* revealed three intensity-modulated phases with a lower energy than AFM-II state [10]. In this study, the ground state at pressures 15–35 GPa was found to be formed by alternating AFM and nonmagnetic bilayers.

At the same time, the *paramagnetic* state of ε-Fe was studied by a combination of DFT and dynamical mean-field theory (DFT+DMFT) [21]. These studies showed the importance of Coulomb correlations for description of the electronic [22,23] and structural [23] properties at moderate pressures, as well as phase stability [3], transport [24–26], and magnetic [3,27] properties at Earth's core conditions. In addition, a jump of resistivity at the $\alpha \rightarrow \varepsilon$ transition was qualitatively captured by Pourovskii *et al.* [23], while quantitative difference was attributed to nonlocal correlation effects (for a review, see Ref. [28]).

The properties of ε-Fe have become even more intriguing with the discovery of superconductivity in the pressure range from 15 to 30 GPa, with the largest critical temperature $T_c = 2$ K at about 21 GPa [29]. The superconducting properties are also unusual. In particular, the superconductivity seems to occur in paramagnetic phase; the large slope of the critical field curve at T_c demonstrates that heavy particles are involved in the pairing (see Ref. [30] and review in Ref. [31]). Moreover, the temperature dependence of resistivity shows a $T^{5/3}$ power-law behavior below 30 K over the entire superconducting pressure region [30,32–36]. This non-Fermi-liquid behavior (in contrast with the T^2 dependence for Fermi liquid) was attributed to ferromagnetic (FM) fluctuations according to Moriya's theory of weak itinerant magnetism [37]. These experimental results point to an unconventional superconductivity; the presence of FM fluctuations may be a signature of triplet pairing symmetry. However, it is at odds with the DFT calculations, predicting a proximity to antiferromagnetism, which would likely yield singlet superconducting state.

A narrow pressure range of superconductivity also suggests that it has a spin-fluctuation origin. This was confirmed by calculations of the electron-phonon coupling within DFT, which showed that the phonon mechanism can explain the appearance of superconductivity in ε-Fe, but not its rapid disappearance with pressure [38,39]. In particular, the calculated range of superconductivity was found to extend well

155126-1

above 100 GPa. To consider the magnetic pairing mechanism, Jarlborg estimated the coupling constant within DFT and concluded that superconductivity mediated by spin fluctuations is more likely than that owing to electron-phonon interaction [40].

Above discussed observations stress the importance of studying correlation effects in ε-iron. In this paper, we study the electronic and magnetic properties of paramagnetic ε-Fe within superconducting pressure range by employing DFT+DMFT approach. We find considerable local correlations, leading to formation of short-lived local magnetic moments, as well as pronounced incommensurate spin fluctuations. To clarify whether these fluctuations can mediate the electron pairing, we derive and solve the multiband Bethe-Salpeter equation (BSE) in the particle-particle channel. The obtained results indicate that the spin fluctuations in ε-Fe may lead to superconducting instability in the experimental pressure range.

The plan of the paper is the following. In Sec. II, we list the computational details. In Sec. III, we present the results on electronic, magnetic and superconducting properties, and finally, in Sect. IV, the conclusions are given. In Appendix, we derive the gap equation and pairing interaction.

II. COMPUTATIONAL DETAILS

We have performed DFT calculations of ε-iron using the full-potential linearized augmented-plane wave method implemented in the ELK code supplemented by the Wannier function projection procedure. The Perdew-Burke-Ernzerhof form of generalized gradient approximation (GGA) was considered. The calculations were carried out with the experimental lattice constants at the corresponding pressures [41]. The convergence threshold for total energy was set to 10^{-6} Ry. The integration in the reciprocal space was performed using $22 \times 22 \times 12$ **k**-point mesh in all calculations except those of the Fermi surface and momentum-dependent susceptibility, where $42 \times 42 \times 22$ mesh was employed. From converged DFT results we have constructed effective Hamiltonians in the basis of Wannier functions, which were built as a projection of the original Kohn-Sham states to site-centered localized functions as described in Ref. [42], considering $3d$, $4s$, and $4p$ states.

In DMFT calculations, we use for d states the Hubbard parameter $U \equiv F^0 = 4.3$ eV and Hund's rule coupling $I = 1.0$ eV, which were used in previous study of ε-Fe and resulted in accurate descriptions of its structural properties at the same pressures as in current work [23]. We note that these values are in overall agreement with estimates for α-iron [43]. Our calculations have been performed using the AMULET code [44]. The double-counting correction has been taken in the around mean-field form. We also verified that the fully localized double-counting correction leads to similar results, although providing a slightly larger ($\sim$0.1) filling of d states. The impurity problem has been solved by the hybridization expansion continuous-time quantum Monte Carlo method [45] with the density-density form of Coulomb interaction. We consider the redistribution of charge density, caused by the self-energy, only within DMFT self-consistency loop. We checked this approximation at several pressures and

temperatures by performing DFT+DMFT calculations both with and without full charge self-consistency, which led to similar results.

We note that the DMFT takes into account local electronic correlations, neglecting the momentum-dependence of self-energy [46]. Although the nonlocal corrections to DMFT can be obtained using cluster [47] or diagrammatic [48] methods, these approaches are too computationally expensive to be applied to real multiorbital compounds at the moment.

III. RESULTS AND DISCUSSION

A. Electronic properties

Within the DFT+DMFT we find the filling of various d orbitals in the range $n = 1.30$–1.36, which is close to the values in α- and γ-iron [49–51], but the peak of the density of states is sufficiently far from the Fermi level (see below). We first analyze possible deviations from the Fermi-liquid (FL) regime by using several criteria employed earlier at Earth's core conditions [3,24]. For brevity, we present the results only for degenerate xy and x^2-y^2 states, while similar results were obtained for z^2 and degenerate xz and yz states.

In a FL state, the imaginary part of self-energy depends linearly on imaginary frequency $i\nu_n$ at small $|\nu_n|$ as $\text{Im}\,\Sigma(i\nu_n) \approx -\Gamma - (Z^{-1}-1)\nu_n$, where Γ is the quasiparticle damping (i.e., inverse quasiparticle lifetime), Z is the quasiparticle residue. In Fig. 1(a), we show the obtained imaginary part of $\Sigma(i\nu_n)$, which scales almost linearly for all considered pressures. To obtain a more quantitative estimate, we compute the quasiparticle damping Γ, which in a FL depends quadratically on temperature, implying $\Gamma/T \propto T$. To this end, we perform the analytical continuation of self-energies by using the Padé approximants [52]. The obtained temperature dependence of Γ/T, shown in the inset of Fig. 1(a), also corresponds to the coherent FL regime.

To obtain an accurate estimate of the temperature T^*, below which the crossover to the FL regime occurs, avoiding use of Padé approximants, we consider the "first Matsubara frequency" rule [53], according to which in the local approximation $\text{Im}\,\Sigma$ at first Matsubara frequency $\nu_1 = \pi T$ does not contain any terms beyond $\mathcal{O}(T)$ in the FL regime. As shown in Fig. 1(b), $\text{Im}\,\Sigma(i\pi T)$ is proportional to temperature below T^* which is $\sim$1500 K at 12 GPa. A gradual increase of T^* with pressure reflects the reduction of the Coulomb correlation strength due to larger bandwidth. These results suggest a possibility of suppression of coherence temperature T^* for larger Hubbard U. However, our calculations with $U = 6$ eV lead to only a weak change of T^*, which is $\sim$1000 K at pressure of 12 GPa [see inset in Fig. 1(b)]. The value of T^* can be also affected by using the full rotationally invariant Coulomb interaction, while the density-density approximation was shown to underestimate the magnitude of scattering $|\text{Im}\,\Sigma(i\nu_n)|$ in ε-Fe [28]. The FL behavior of ε-Fe was also predicted by Pourovskii *et al.* at Earth's core conditions [3,24], even at the relatively high temperature of $\sim$6000 K, while a contrary conclusion was obtained by Zhang *et al.* [26].

The Coulomb correlations in ε-Fe result in substantial mass enhancement $m^*/m = Z^{-1}$, which, averaged over all d orbitals, is equal to 1.8 at 12 GPa and gradually decreases to
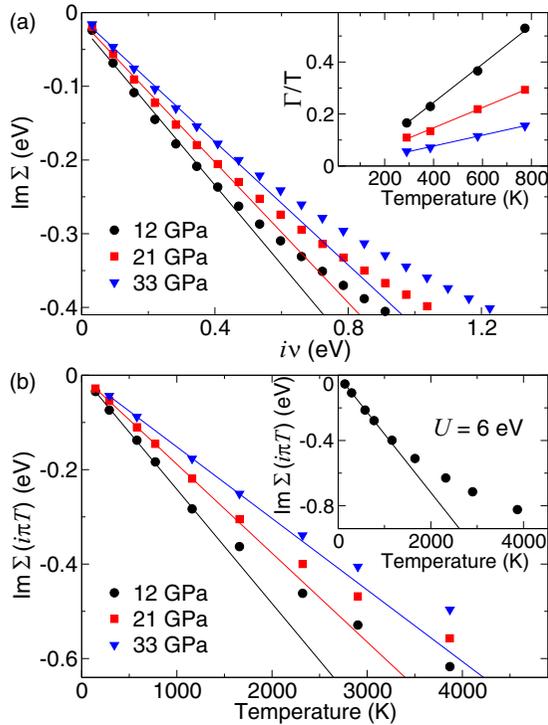
FIG. 1. (a) Imaginary part of self-energy for degenerate xy and x^2-y^2 states as a function of imaginary frequency $i\nu$ obtained by DFT+DMFT method at $\beta = 100 \, \text{eV}^{-1}$. (Inset) Temperature dependence of the ratio of quasiparticle damping Γ to temperature T. (b) Imaginary part of the above mentioned self-energy at the first Matsubara frequency as a function of temperature. (Inset) The same for $U = 6$ eV. The straight lines depict the fit to linear dependence.

1.55 at 33 GPa in agreement with earlier studies [23]. The enhancement of the quasiparticle mass is accompanied by the renormalization of the density of states (DOS) near the Fermi level as displayed in Fig. 2. As a result, the distance from the peak lying above the Fermi level is decreased to 0.4 eV compared to 0.75 eV obtained in DFT calculations at 12 GPa. The DOS at the Fermi level decreases with pressure, but not
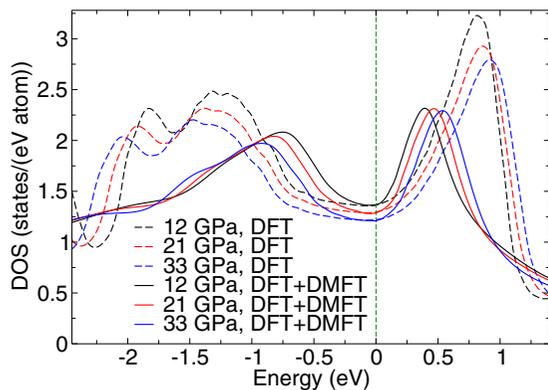

FIG. 2. Density of states of ε-Fe obtained within DFT and DFT+DMFT at $T = 290$ K for different pressures. The Fermi level is at zero energy.
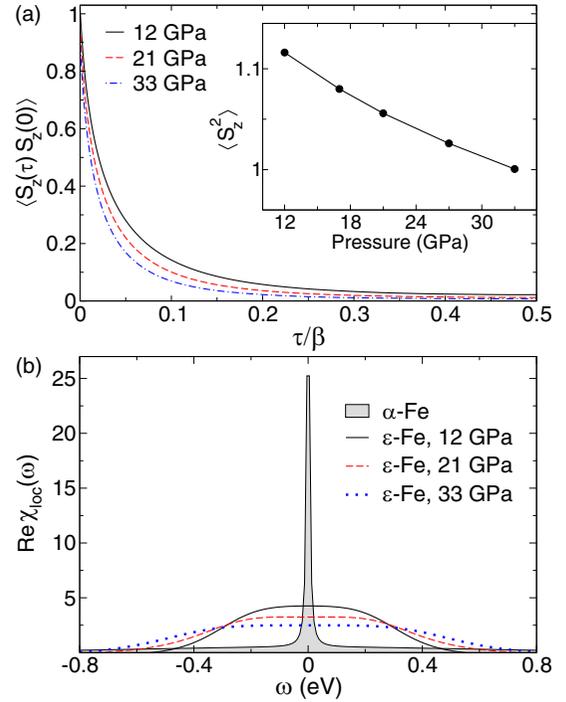

FIG. 3. Local spin-spin correlation functions in the imaginary-time (a) and real-energy (b) domains calculated by DFT+DMFT method at $\beta = 40 \, \text{eV}^{-1}$. In the bottom panel, the obtained correlation functions are compared with that for α-Fe [54]. (Inset) Instantaneous average $\langle S_z^2 \rangle$ for ε-Fe as a function of pressure.

rapidly enough to explain the disappearance of superconductivity, as was also noted previously [38].

B. Magnetic properties

In Fig. 3(a), we present the local spin-spin correlation functions $\langle S_z(\tau)S_z(0) \rangle$ at $T = 290$ K, which have a significant instantaneous average $\langle S_z^2 \rangle \simeq 1$, and decay rapidly with imaginary time τ. This τ dependence corresponds to fast quantum fluctuations of instantaneous magnetic moments on lattice sites. To estimate the degree of spin localization, we Fourier transform the spin correlator to imaginary bosonic frequencies, $\chi_{\text{loc}}(i\omega_n) = \int_0^\beta \exp(i\omega_n\tau)\langle S_z(\tau)S_z(0)\rangle$, and then analytically continue it to real frequency ω. The real part of the obtained $\chi_{\text{loc}}(\omega)$ is shown in Fig. 3(b) in comparison with that of α-iron [54] (see also Refs. [49–51]), being a system with well-defined local moments. The half width of the peak in $\text{Re}\,\chi_{\text{loc}}(\omega)$ at half of its height yields approximately inverse lifetime of local magnetic moments [50]. For ε-iron, we therefore obtain the inverse lifetime in energy units ranging from 0.3 eV at $p = 12$ GPa to 0.5 eV at $p = 33$ GPa, which corresponds to the lifetime of local moments ranging from 14 to 8 fs, respectively. This is comparable to the lifetime of local moments, discussed previously in pnictides [55]. Thus the obtained results show a presence of short-lived local magnetic moments, which lifetime decreases with increasing pressure in agreement with XES measurements [10,13,14].

To get further insight into the formation of local moments, we calculate the uniform magnetic susceptibility as a response
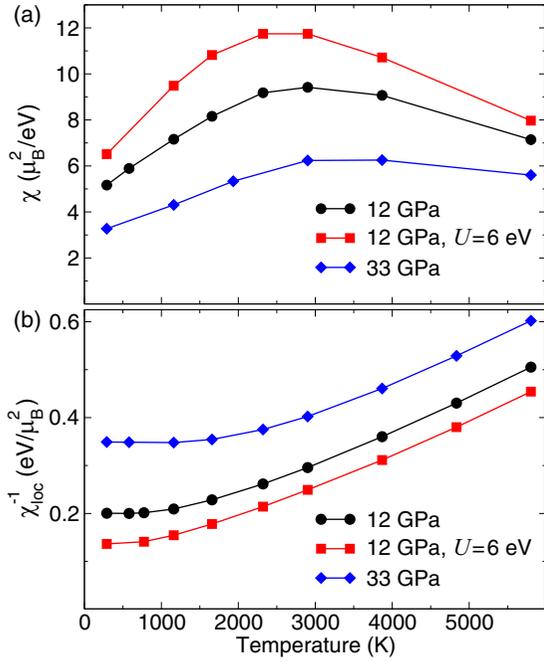
FIG. 4. Temperature dependence of uniform magnetic susceptibility (a) and inverse local susceptibility (b) for ε-Fe obtained within DFT+DMFT method.

FIG. 5. Momentum-dependence of the particle-hole bubble obtained within DFT and DFT+DMFT at $\beta = 100$ eV^{-1}.

(DFT+DMFT) propagators. In both cases, $\chi_{\mathbf{q}}^0$ has a similar shape with a maximum at incommensurate wave vector, lying near K and M points of the Brillouin zone. These preferable wave vectors are in agreement with previous DFT analysis [18–20]. The particle-hole bubble increases with decreasing pressure due to decrease of the bandwidth. Therefore both uniform and nonuniform spin fluctuations become stronger with decreasing pressure.

C. Superconducting pairing

To study possible symmetries of electron pairing, we consider simplified approach, using pairing interaction vertex $V_{\mathbf{k}\mathbf{k}',\alpha\beta}^{s,t}$ (α, β are band indices and $\mathbf{k}$, $\mathbf{k}'$ are the respective momenta) in the singlet (s) and triplet (t) channels, obtained in the second order of perturbation theory, similarly to the original Kohn and Luttinger paper [60], see also Refs. [61,62] and Appendix. Although the Coulomb interaction in ε-iron is not small, we expect that this approach correctly reproduces the symmetry of the gap function, in view of the Fermi-liquid behavior of electronic self-energies at low temperatures, obtained in Sec. III A. For more sophisticated approaches, accounting for higher-order diagrams, e.g., in a ladder series [63–65], in the presence of strong electronic correlations, it is preferable considering dynamic vertices [48] instead of static ones, which requires introducing Moriyaesque lambda correction [66] and/or treating nonlocal self-energy feedback [64] to avoid unphysical divergences of the series. Such generalizations previously were explored for the single-band models only (see, e.g., Refs. [64,65]). For the considering multiband models, they are rather tedious and not performed here.

To determine pairing symmetry, we consider eigenvalues $\lambda^{s,t}$ and eigenfunctions $f_{\mathbf{k},\alpha}^{s,t}$ of the Bethe-Salpeter equation

$$\lambda^{s,t} f_{\mathbf{k},\alpha}^{s,t} = -\sum_{\mathbf{k}',i\nu_n,\beta} V_{\mathbf{k}\mathbf{k}',\alpha\beta}^{s,t} f_{\mathbf{k}'\beta}^{s,t} G_{\mathbf{k}'\beta}(i\nu_n) G_{\mathbf{k}'\beta}(-i\nu_n), \quad (2)$$

where $G_{\mathbf{k}\alpha}(i\nu_n)$ is the Green function for the band α, obtained by the diagonalization of the Green functions matrices $G_{\mathbf{k}}(i\nu_n)$ with respect to orbital indexes. We parametrize the gap functions $f_{\mathbf{k},\alpha}$ for momenta lying on the Fermi surface and assume them to be independent on the radial direction

to a small external magnetic field introduced in the DMFT part [see Fig. 4(a)]. In particular, we have used the magnetic field corresponding to splitting of the single-electron energies by 0.02 eV, which was checked to provide a linear response. The calculated uniform susceptibility, shown in Fig. 4(a), increases almost linearly with temperature at low temperatures and decrease above a certain temperature $\sim$3000 K, determined by the distance from the peak of the density of states to the Fermi level, similarly to other systems with a peak of the density of states shifted off the Fermi level [50,56]. Increasing value of U leads to increase of uniform susceptibility.

The static local spin susceptibility $\chi_{\text{loc}} = 4\mu_B^2 \chi_{\text{loc}}(0)$ shows a Pauli-like behavior below the temperature T^* of a crossover to the Fermi liquid regime and a Curie-Weiss behavior $\chi_{\text{loc}} \propto (T - T_{\text{loc}})^{-1}$ above T^* due to presence of the unscreened local moments [see Fig. 4(b)]. The "Weiss" temperature T_{loc} is negative and determines the Kondo temperature $T_K \sim -T_{\text{loc}}$ below which the local moments are screened by conduction electrons, similarly to the single-impurity Kondo model [57–59], for which $T_K \approx -T_{\text{loc}}/\sqrt{2}$. We find $T_{\text{loc}} \sim -T^*$ and therefore rather large Kondo temperatures $T_K \sim T^*$. Similarly to T^*, the Kondo temperature is somewhat suppressed at $U = 6$ eV.

Next we calculate the particle-hole bubble

$$\chi_{\mathbf{q}}^0 = -\left(2\mu_B^2/\beta\right) \sum_{\mathbf{k},\nu_n} \text{Tr}[G_{\mathbf{k}}(i\nu_n) G_{\mathbf{k}+\mathbf{q}}(i\nu_n)], \quad (1)$$

where $G_{\mathbf{k}}(i\nu_n)$ is the one-particle Green function, which is a matrix in the d-orbital space, obtained using the Wannier-projected Hamiltonian and ν_n are the Matsubara frequencies. In Fig. 5, we show the momentum dependence of $\chi_{\mathbf{q}}^0$ calculated using noninteracting (DFT) and interacting
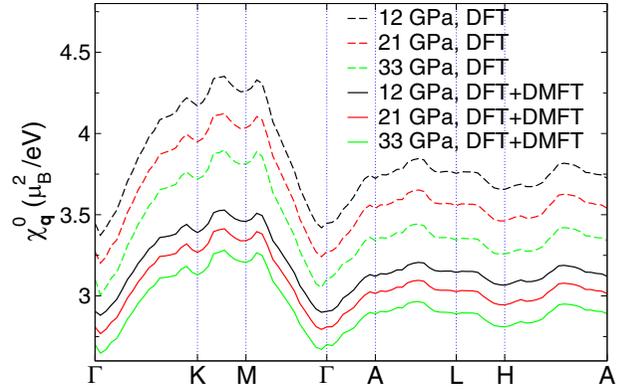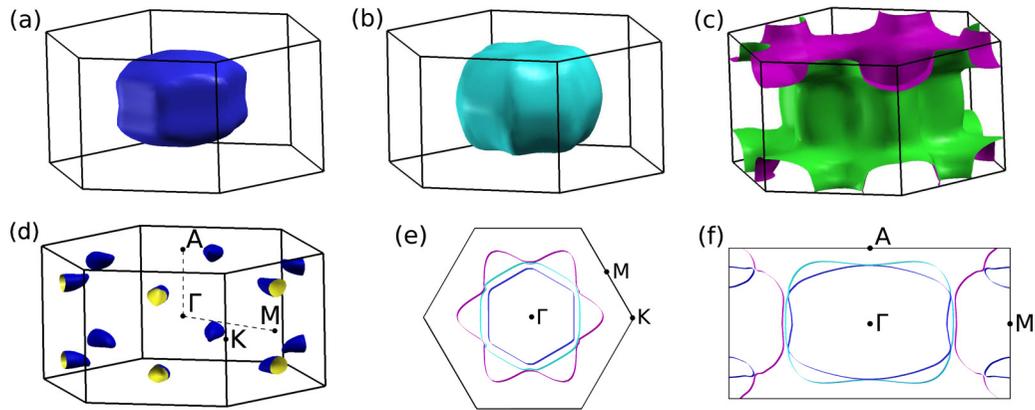
FIG. 6. Fermi surface sheets of ε-Fe obtained by DFT+DMFT at 12 GPa [(a)–(d)]. Plots (e) and (f) show cuts of the Fermi surface sheets by the planes passing through points M, Γ, K and M, Γ, A, respectively. The line width has no meaning.

of **k**, since the summation in Eq. (2) is anyhow dominated by the vicinity of the Fermi surface. Among many sheets of the Fermi surface (see Fig. 6), we choose the two most important [Figs. 6(a) and 6(b)], which parts are connected by nesting vectors. We parametrize points of these Fermi surface sheets by the polar and azimuthal angles (θ, ϕ), where $\phi = 0$ corresponds to point M of the Brillouin zone, $\theta = 0, \pi$ to the "north" and "south" poles.

The largest (leading) eigenvalue determines the preferred momentum dependence of the pairing gap, given by the corresponding eigenfunction [67,68]. Calculated leading eigenvalues of singlet and triplet pairing are shown in Fig. 7. For the considered range of pressures, singlet and triplet eigenvalues are close to each other. Interestingly, we obtain crossing of eigenvalues of singlet and triplet pairing near the pressure $p_c = 22$ GPa, close to that, at which maximum value of superconducting T_c is obtained. Yet, both eigenvalues increase with decreasing pressure, so that the obtained pressure dependence agrees with the experimental data for $p > p_c$. For $p < p_c$, the considered theory does not describe the suppression of superconductivity with decreasing pressure. The increase of the eigenvalues with decreasing pressure, however, goes along with the increase of the nonuniform susceptibility, see Fig. 5
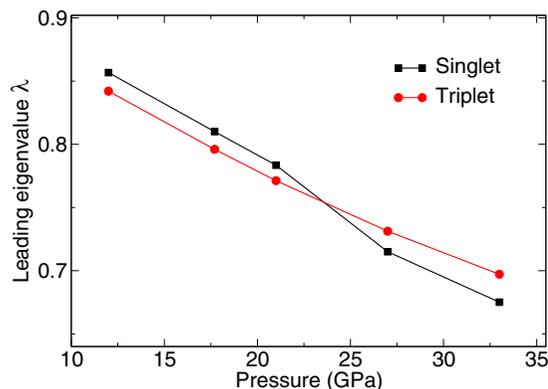
and shows the spin-fluctuation origin of the obtained superconducting order parameters. We note that the obtained close competition of singlet and triplet pairing is similar to that discussed previously for Sr_2RuO_4 (see, e.g., Refs. [62,69]) and may be lifted by going beyond second-order perturbation theory, including nearest-neighbor Coulomb repulsion, spin-orbit coupling etc.

Obtained momentum dependence of the gap functions for singlet order parameters [Figs. 8(a) and 8(b)] take the values $\approx 0, \pm\Delta$ at the subsequent vertical faces of the considered Fermi surface sheets. This momentum dependence allows one to achieve a change of the sign of gap function on the opposite sides of the Fermi surface, connected by the wave vector of preferred incommensurate fluctuations in the K-M direction. On the contrary, the triplet pairing gap is almost ϕ-independent and changes sign at $\theta = \pi/2$, having a single line of the nodes.

IV. CONCLUSIONS

We have studied electronic and magnetic properties of ε-Fe at pressures up to 33 GPa by employing the DFT+DMFT approach and using its results as a starting point for the multiband Bethe-Salpeter equation. Our main results are as follows.

(i) We have not found a significant deviation from the FL behavior below 1000 K even with relatively large $U = 6$ eV. This points to the importance of nonlocal correlations effects, neglected in DMFT.

(ii) At the same time, the Coulomb correlations lead to substantial electron mass enhancement up to $m^*/m \sim 1.8$, which is accompanied by renormalization of the density of states. As a result, the distance from the peak lying above the Fermi level is decreased to 0.4 eV compared to 0.75 eV obtained in DFT calculations.

(iii) We have found short-lived magnetic moments with the lifetime ~ 10 fs, comparable to that estimated previously in pnictides. This may explain the discrepancy of XES experiments with the Mössbauer spectroscopy because of the longer time scales of the latter. Namely, the lifetime of local magnetic moments or spin fluctuations
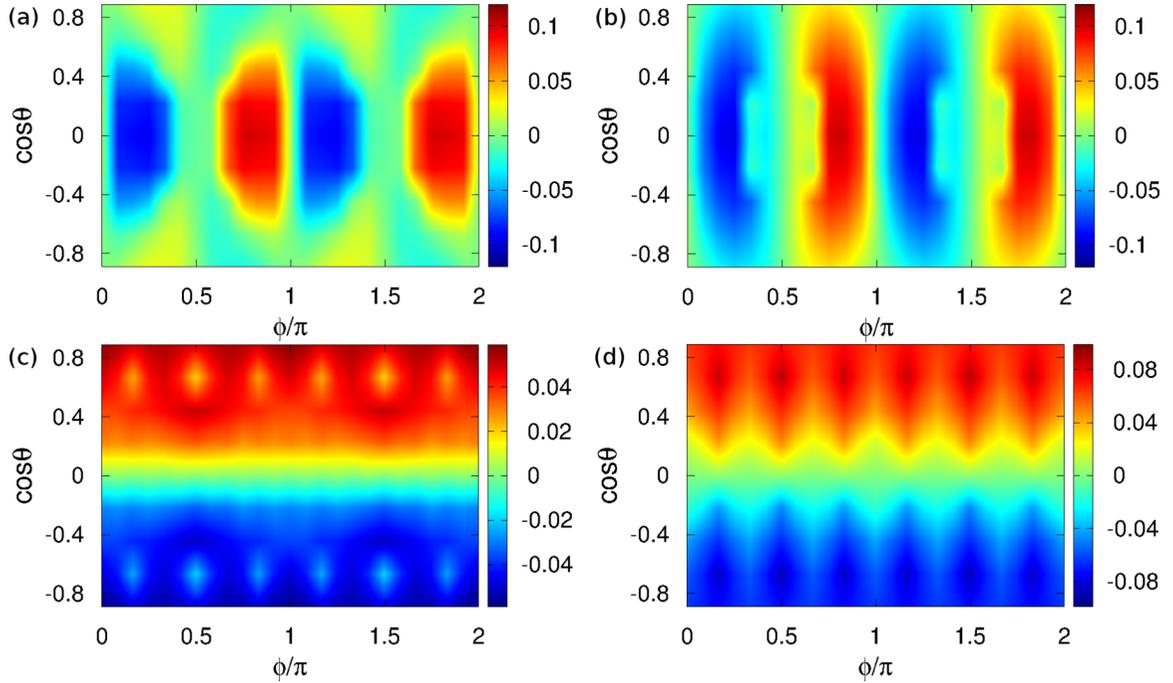

FIG. 7. Leading eigenvalue of the Bethe-Salpeter equation for singlet and triplet pairing in ε-Fe calculated at $\beta = 100$ eV^{-1}.

FIG. 8. Eigenfunction of the Bethe-Salpeter equation for singlet [(a) and (b)] and triplet [(c) and (d)] pairing as a function of polar θ and azimuthal ϕ angles calculated at pressure of 21 GPa and $\beta = 100$ eV^{-1}. (a), (c) and (b), (d) correspond to sheets of Fermi surface depicted in Figs. 6(a) and 6(b), respectively. Angle $\phi = 0$ corresponds to point M of the Brillouin zone.

can be small enough to be undetected by the Mössbauer measurements.

(iv) We find that the antiferromagnetic spin fluctuations are the dominant ones. At the same time, we do not find substantial ferromagnetic correlations responsible for the $T^{5/3}$ dependence of the resistivity. This indicates that the nonlocal correlation effects beyond DMFT may play a significant role in ε-Fe. In particular, nonlocal correlation effects corresponding to virtual transitions into a peak lying near the Fermi level may give a contribution [70]. For this contribution, the peak needs not to lie directly at E_F; moreover, its distance from E_F needs not to be too small.

(v) The antiferromagnetic spin fluctuations in ε-Fe can result in the superconducting instability. The obtained results allow us to explain the appearance of superconducting instability in the considered temperature range and its disappearance with pressure, but not a gradual grow of the superconducting critical temperature T_c from 15 to 21 GPa. The growth of T_c with pressure in the low-pressure range may be explained by earlier suggested [40] presence of magnetic clusters of α phase within ε phase, which both are metastable in a wide pressure range. These magnetic clusters, more common at low pressures, or, alternatively, other lattice defects can affect the electron pairing, leading to suppression of the critical temperature. The latter explanation is supported by the experimental fact that $\alpha \to \varepsilon$ martensitic transition is sluggish, and pressures higher than 20 GPa are needed for a complete transformation [32,71].

As it follows from the above discussion, further study of the nonlocal correlations in ε-iron seems to be important. This would allow studying in more detail mechanism of superconductivity and its pressure dependence, and may allow to explain observed $T^{5/3}$ behavior of resistivity, accompanied by

a quantum phase transition at the pressure $p = 21$ GPa [36]. On the other hand, further experimental studies are required to clarify the magnetic and superconducting properties of ε-Fe, that may also have significant implications for geophysics and Earth's core magnetism.

APPENDIX: SUPERCONDUCTING PAIRING

1. General formalism and the gap equation

We consider the general form of the noninteracting Hamiltonian

$$\hat{H}_0 = \sum_{\mathbf{k}\sigma} \sum_{mm'} \varepsilon_{\mathbf{k}}^{mm'} c_{\mathbf{k},m\sigma}^{\dagger} c_{\mathbf{k},m\sigma} \tag{A1}$$

and 4-fermion interaction

$$\hat{H}_{\text{int}} = -\frac{1}{4} \sum_{\sigma\sigma'\sigma''\sigma'''} \sum_{mm'm''m'''} \sum_{\mathbf{k}_1\mathbf{k}_2\mathbf{k}_3\mathbf{k}_4} \Gamma_{\mathbf{k}_1,\mathbf{k}_2;\mathbf{k}_3,\mathbf{k}_4}^{\sigma\sigma'\sigma''\sigma''',mm'm''m'''} c_{\mathbf{k}_1,m\sigma}^{\dagger}$$

$$\times c_{\mathbf{k}_2,m'\sigma'}^{\dagger} c_{\mathbf{k}_3,m''\sigma''} c_{\mathbf{k}_4,m'''\sigma'''} \delta(\mathbf{k}_1 + \mathbf{k}_2 - \mathbf{k}_3 - \mathbf{k}_4), \tag{A2}$$

where m, m', m'', m''' are the orbital indexes, σ, σ', σ'', $\sigma''' = \uparrow, \downarrow$ are the spin indexes, $c_{\mathbf{k}m\sigma}$ are the fermionic operators. Due to the Pauli principle, the interaction

vertex Γ is antisymmetric:

$$\Gamma^{\sigma\sigma'\sigma''\sigma''',mm'm''m'''}_{\mathbf{k}_1,\mathbf{k}_2;\mathbf{k}_3,\mathbf{k}_4} = V^{mm'm''m'''}_{\mathbf{k}_1,\mathbf{k}_2;\mathbf{k}_3,\mathbf{k}_4}\delta_{\sigma\sigma''}\delta_{\sigma'\sigma'''} - V^{mm'm''m'''}_{\mathbf{k}_1,\mathbf{k}_2;\mathbf{k}_4,\mathbf{k}_3}\delta_{\sigma\sigma'''}\delta_{\sigma'\sigma''} \tag{A3a}$$

$$V^{mm'm''m'''}_{\mathbf{k}_1,\mathbf{k}_2;\mathbf{k}_3,\mathbf{k}_4} = V^{m'm,m'''m''}_{\mathbf{k}_2,\mathbf{k}_1;\mathbf{k}_4,\mathbf{k}_3} = \left(V^{m''m''',mm'}_{\mathbf{k}_3,\mathbf{k}_4;\mathbf{k}_1,\mathbf{k}_2}\right)^*, \tag{A3b}$$

where for SU(2) symmetric interaction the vertices V do not depend on spin indexes.

To discuss superconducting pairing, we perform the mean-field decoupling

$$\hat{H}_{\text{int}} \to \hat{H}^{\text{BCS}}_{\text{int}} = -\frac{1}{4}\sum_{\mathbf{kp},mm',m''m'''}\sum_{\sigma\sigma'\sigma''\sigma'''}\left[\Gamma^{\sigma\sigma'\sigma''\sigma''',mm'm''m'''}_{\mathbf{k},-\mathbf{k};\mathbf{p},-\mathbf{p}}c^\dagger_{\mathbf{k},m\sigma}c^\dagger_{-\mathbf{k},m'\sigma'}\langle c_{\mathbf{p},m''\sigma''}c_{-\mathbf{p},m'''\sigma'''}\rangle + \text{h.c.}\right]. \tag{A4}$$

We suppose that the quadratic part $\hat{H}_0$ of the Hamiltonian is diagonalized by the transformation $c_{\mathbf{p},m\sigma} = \sum_\alpha U^{m\alpha}_{\mathbf{p}}e_{\mathbf{p},\alpha\sigma}$, where $e_{\mathbf{k},\alpha\sigma}$ are the fermionic operators for the band α and spin projection σ, such that

$$\hat{H}_0 = \sum_{\mathbf{k}\alpha\sigma}\epsilon_{\mathbf{k}\alpha}e^\dagger_{\mathbf{k},\alpha\sigma}e_{\mathbf{k},\alpha\sigma}, \tag{A5}$$

where $E_{\mathbf{k}\alpha} = \sum_{mm'}\varepsilon^{mm'}_{\mathbf{k}}(U^{m\alpha}_{\mathbf{k}})^*U^{m'\alpha}_{\mathbf{k}}$, $\sum_{mm'}\varepsilon^{mm'}_{\mathbf{k}}(U^{m\alpha}_{\mathbf{k}})^*U^{m'\beta}_{\mathbf{k}} = 0$ $(\alpha \neq \beta)$. Then we obtain

$$\hat{H}^{\text{BCS}}_{\text{int}} = -\frac{1}{4}\sum_{\mathbf{kp}}\sum_{\sigma\sigma'\sigma''\sigma''',\alpha\beta}\left[\Gamma^{\sigma\sigma'\sigma''\sigma''',\alpha\beta}_{\mathbf{k},\mathbf{p}}e^\dagger_{\mathbf{k},\alpha\sigma}e^\dagger_{-\mathbf{k},\alpha\sigma'}\langle e_{\mathbf{p},\beta\sigma''}e_{-\mathbf{p},\beta\sigma'''}\rangle + \text{H.c.}\right]$$

$$= \frac{1}{2}\sum_{\mathbf{k}\alpha,\sigma\sigma'}\left[\Delta^{\sigma\sigma'}_{\mathbf{k},\alpha}e^\dagger_{\mathbf{k},\alpha\sigma}e^\dagger_{-\mathbf{k},\alpha\sigma'} + \text{H.c.}\right], \tag{A6}$$

where

$$\Delta^{\sigma,\sigma'}_{\mathbf{k},\alpha} = -\frac{1}{2}\sum_{\mathbf{p},\sigma''\sigma''',\beta}\Gamma^{\sigma\sigma'\sigma''\sigma''',\alpha\beta}_{\mathbf{k},\mathbf{p}}\langle e_{\mathbf{p},\beta\sigma''}e_{-\mathbf{p},\beta\sigma'''}\rangle \tag{A7}$$

and

$$\Gamma^{\sigma\sigma'\sigma''\sigma''',\alpha\beta}_{\mathbf{k},\mathbf{p}} = \sum_{mm',m''m'''}\Gamma^{\sigma\sigma'\sigma''\sigma''',mm'm''m'''}_{\mathbf{k},-\mathbf{k};\mathbf{p},-\mathbf{p}}\left(U^{m\alpha}_{\mathbf{k}}\right)^*\left(U^{m'\alpha}_{-\mathbf{k}}\right)^*U^{m''\beta}_{\mathbf{p}}U^{m'''\beta}_{-\mathbf{p}}. \tag{A8}$$

As usually, we separate singlet and triplet terms:

$$\Delta^{\sigma,\sigma'}_{\mathbf{k},\alpha} = -\Delta^{\sigma',\sigma}_{-\mathbf{k},\alpha} = \left(\Delta^{\sigma,\sigma'}_{\mathbf{k},\alpha}\right)_s + \left(\Delta^{\sigma,\sigma'}_{\mathbf{k},\alpha}\right)_t,$$

$$\left(\Delta^{\sigma,\sigma'}_{\mathbf{k},\alpha}\right)_s = \left(\Delta^{\sigma,\sigma'}_{-\mathbf{k},\alpha}\right)_s = -\left(\Delta^{\sigma',\sigma}_{\mathbf{k},\alpha}\right)_s = i\sigma^{\sigma\sigma'}_y\psi_{\mathbf{k},\mu} = \begin{pmatrix} 0 & \psi_{\mathbf{k},\alpha} \\ -\psi_{\mathbf{k},\alpha} & 0 \end{pmatrix}_{\sigma\sigma'};$$

$$\left(\Delta^{\sigma,\sigma'}_{\mathbf{k},\alpha}\right)_t = -\left(\Delta^{\sigma,\sigma'}_{-\mathbf{k},\alpha}\right)_t = \left(\Delta^{\sigma',\sigma}_{\mathbf{k},\alpha}\right)_t = i(\mathbf{d}_{\mathbf{k},\mu}\boldsymbol{\sigma}^{\sigma\sigma''})\sigma^{\sigma''\sigma'}_y = \begin{pmatrix} -d^x_{\mathbf{k},\alpha} + id^y_{\mathbf{k},\alpha} & d^z_{\mathbf{k},\alpha} \\ d^z_{\mathbf{k},\alpha} & d^x_{\mathbf{k},\alpha} + id^y_{\mathbf{k},\alpha} \end{pmatrix}_{\sigma\sigma'}. \tag{A9}$$

where $\boldsymbol{\sigma}$ are the Pauli matrices. From these relations, we find

$$\left(\Delta^{\sigma,\sigma'}_{\mathbf{k},\alpha}\right)_{s(t)} = \frac{1}{2}\left(\Delta^{\sigma,\sigma'}_{\mathbf{k},\alpha} \mp \Delta^{\sigma',\sigma}_{\mathbf{k},\alpha}\right) = -\frac{1}{2}\sum_{\mathbf{p},\sigma''\sigma''',\beta}\Gamma^{\sigma\sigma'\sigma''\sigma''',\alpha\beta}_{s(t),\mathbf{k},\mathbf{p}}\langle e_{\mathbf{p},\beta\sigma''}e_{-\mathbf{p},\beta\sigma'''}\rangle$$

$$= -\sum_{\mathbf{p},\beta}V^{s(t)}_{\mathbf{kp},\alpha\beta}\langle e_{\mathbf{p},\beta\sigma}e_{-\mathbf{p},\beta\sigma'}\rangle, \tag{A10}$$

where

$$\Gamma^{\sigma\sigma'\sigma''\sigma''',\alpha\beta}_{s(t),\mathbf{k},\mathbf{p}} = \frac{1}{2}\left(\Gamma^{\sigma\sigma'\sigma''\sigma''',\alpha\beta}_{\mathbf{k},\mathbf{p}} \mp \Gamma^{\sigma'\sigma\sigma''\sigma''',\alpha\beta}_{\mathbf{k},\mathbf{p}}\right), \tag{A11}$$

$$V^{s(t)}_{\mathbf{k},\mathbf{p},\alpha\beta} = \frac{1}{2}\sum_{mm',m''m'''}\left(V^{mm'm''m'''}_{\mathbf{k},-\mathbf{k};\mathbf{p},-\mathbf{p}} \pm V^{mm'm'''m''}_{\mathbf{k},-\mathbf{k};-\mathbf{p},\mathbf{p}}\right)\left(U^{m\alpha}_{\mathbf{k}}\right)^*\left(U^{m'\alpha}_{-\mathbf{k}}\right)^*U^{m''\beta}_{\mathbf{p}}U^{m'''\beta}_{-\mathbf{p}}. \tag{A12}$$

From Eq. (A10), we obtain gap equations:

$$\psi_{\mathbf{k},\alpha} = -\sum_{\mathbf{k}',iv'_n,\beta}V^s_{\mathbf{kk}',\alpha\beta}F^s_{\mathbf{k}'\beta}(iv'_n), \tag{A13a}$$

$$\mathbf{d}_{\mathbf{k},\alpha} = -\sum_{\mathbf{k}',iv'_n,\beta}V^t_{\mathbf{k},\mathbf{k}',\alpha\beta}\mathbf{F}^t_{\mathbf{k}'\beta}(iv'_n), \tag{A13b}$$

where $F_{\mathbf{k}\alpha}^s(iv_n) = (i\sigma_y^{\sigma\sigma'}/2)\langle e_{\mathbf{k}\alpha\sigma}(\tau)e_{\mathbf{k}\alpha\sigma'}(0)\rangle_{iv_n}$ and $\mathbf{F}_{\mathbf{k}\alpha}^t(iv_n) = (i/2)(\boldsymbol{\sigma}\sigma_y)^{\sigma\sigma'}\langle e_{\mathbf{k}\alpha\sigma}(\tau)e_{\mathbf{k}\alpha\sigma'}(0)\rangle_{iv_n}$ are the anomalous Green functions of the Hamiltonian $\hat{H}_0 + \hat{H}_{\text{int}}^{\text{BCS}}$, the index iv_n denotes the Fourier transform. The corresponding Bethe-Salpeter equations are obtained by linearizing the gap equations and considering the eigenvalues and eigenfunctions of the operators in the right-hand side of Eq. (A13), see Eq. (2) of the main text.

2. Bare and second-order vertex

To determine the vertex V, we use the second-order perturbation theory. To preserve spin-rotational symmetry, we consider the following orbital-dependent interactions:

$$H_{\text{int}} = U \sum_{im} n_{im\uparrow}n_{im\downarrow} + \sum_{i,m>m',\sigma} U_1^{mm'} n_{im\sigma}n_{im'\sigma} + \sum_{i,m>m',\sigma} U_2^{mm'} n_{im\sigma}n_{im',-\sigma}$$
$$+ \sum_{i,m>m',\sigma\sigma'} (U_2^{mm'} - U_1^{mm'})c_{im\sigma}^+ c_{im,-\sigma}c_{im'-\sigma}^+ c_{im'\sigma} + \sum_{i,m\neq m'} J^{mm'} c_{im\uparrow}^+ c_{im,\downarrow}^+ c_{im',\downarrow}c_{im',\uparrow} \tag{A14}$$

(for the standard Kanamori parametrization with Hund exchange I, interorbital exchange $U' - I/2$, and pair hopping J we have $U_2^{mm'} = U'$, $U_1^{mm'} = U' - I$, $J^{mm'} = J$). For the bare local vertex $V_0^{mm'm''m'''}$ defined by putting the Hamiltonian (A14) into the form of Eqs. (A2) and (A3a), we have

$$V_0^{mm',m''m'''} = U\delta_{mm''}\delta_{m'm'''}\delta_{mm'} + U_2^{mm'}\delta_{mm''}\delta_{m'm'''}(1 - \delta_{mm'})$$
$$+ (U_2^{mm'} - U_1^{mm'})\delta_{mm'''}\delta_{m'm''}(1 - \delta_{mm'}) + J^{mm'}\delta_{mm'}\delta_{m''m'''}(1 - \delta_{mm''}). \tag{A15}$$

In the second order in V_0, the effective interaction is given by $V_0^{mm'm''m'''} + V_{2,\mathbf{k},-\mathbf{k};\mathbf{p},-\mathbf{p}}^{mm'm''m'''}$, where

$$V_{2,\mathbf{k},-\mathbf{k};\mathbf{p},-\mathbf{p}}^{mm'm''m'''} = L_{ph}^{\tilde{m}''\tilde{m}''',\tilde{m}'\tilde{m}}(\mathbf{k}-\mathbf{k})\big[-2V_0^{m\tilde{m},m''\tilde{m}'}V_0^{\tilde{m}'m',\tilde{m}''m'''}$$
$$+ V_0^{m\tilde{m},m''\tilde{m}''}V_0^{\tilde{m}'m',m''\tilde{m}'''}\big] + L_{ph}^{\tilde{m}\tilde{m},\tilde{m}''\tilde{m}'''}(\mathbf{k}+\mathbf{p})V_0^{m\tilde{m}''',\tilde{m}mm''}V_0^{\tilde{m}'m',m''\tilde{m}'}, \tag{A16}$$

where we assume summation over repeating orbital indices and

$$L_{ph}^{mm',m''m'''}(\mathbf{q}) = -T \sum_{\mathbf{k},iv_n} G_{\mathbf{k}}^{mm''}(iv_n)G_{\mathbf{k}+\mathbf{q}}^{m'm'''}(iv_n) \tag{A17}$$

is the particle-hole bubble.

---

[1] T. Takahashi and W. A. Bassett, Science **145**, 483 (1964).

[2] S. Tateno, K. Hirose, Y. Ohishi, and Y. Tatsumi, Science **330**, 359 (2010).

[3] L. V. Pourovskii, T. Miyake, S. I. Simak, A. V. Ruban, L. Dubrovinsky, and I. A. Abrikosov, Phys. Rev. B **87**, 115130 (2013).

[4] A. Hausoel, M. Karolak, E. Şaşıoğlu, A. Lichtenstein, K. Held, A. Katanin, A. Toschi, and G. Sangiovanni, Nat. Commun. **8**, 16062 (2017).

[5] G. Cort, R. D. Taylor, and J. O. Willis, J. Appl. Phys. **53**, 2064 (1982).

[6] R. D. Taylor, G. Cort, and J. O. Willis, J. Appl. Phys. **53**, 8199 (1982).

[7] S. Nasu, T. Sasaki, T. Kawakami, T. Tsutsui, and S. Endo, Phys. Condens. Matter **14**, 11167 (2002).

[8] A. B. Papandrew, M. S. Lucas, R. Stevens, I. Halevy, B. Fultz, M. Y. Hu, P. Chow, R. E. Cohen, and M. Somayazulu, Phys. Rev. Lett. **97**, 087202 (2006).

[9] O. Mathon, F. Baudelet, J. P. Itié, A. Polian, M. d'Astuto, J. C. Chervin, and S. Pascarelli, Phys. Rev. Lett. **93**, 255503 (2004).

[10] B. W. Lebert, T. Gorni, M. Casula, S. Klotz, F. Baudelet, J. M. Ablett, T. C. Hansen, A. Juhin, A. Polian, P. Munsch *et al.*, Proc. Natl. Acad. Sci. USA **116**, 20280 (2019).

[11] S. Merkel, A. Goncharov, H. Mao, P. Gillet, and R. Hemley, Science **288**, 1626 (2000).

[12] A. F. Goncharov and V. V. Struzhkin, J. Raman Spectrosc. **34**, 532 (2003).

[13] J.-P. Rueff, M. Mezouar, and M. Acet, Phys. Rev. B **78**, 100405(R) (2008).

[14] A. Monza, A. Meffre, F. Baudelet, J.-P. Rueff, M. d'Astuto, P. Munsch, S. Huotari, S. Lachaize, B. Chaudret, and A. Shukla, Phys. Rev. Lett. **106**, 247201 (2011).

[15] G. Steinle-Neumann, L. Stixrude, and R. E. Cohen, Phys. Rev. B **60**, 791 (1999).

[16] G. Steinle-Neumann, R. E. Cohen, and L. Stixrude, J. Phys.: Condens. Matter **16**, S1109 (2004).

[17] M. Friák, and M. Šob, Phys. Rev. B **77**, 174117 (2008).

[18] G. Steinle-Neumann, L. Stixrude, and R. E. Cohen, Proc. Natl. Acad. Sci. USA **101**, 33 (2004).

[19] V. Thakor, J. B. Staunton, J. Poulter, S. Ostanin, B. Ginatempo, and E. Bruno, Phys. Rev. B **67**, 180405(R) (2003).

[20] R. Lizárraga, L. Nordström, O. Eriksson, and J. Wills, Phys. Rev. B **78**, 064410 (2008).

[21] V. I. Anisimov, A. I. Poteryaev, M. A. Korotin, A. O. Anokhin, and G. Kotliar, J. Phys.: Condens. Matter **9**, 7359 (1997);

A. I. Lichtenstein and M. I. Katsnelson, Phys. Rev. B **57**, 6884 (1998).

[22] K. Glazyrin, L. V. Pourovskii, L. Dubrovinsky, O. Narygina, C. McCammon, B. Hewener, V. Schünemann, J. Wolny, K. Muffler, A. I. Chumakov *et al.*, Phys. Rev. Lett. **110**, 117206 (2013).

[23] L. V. Pourovskii, J. Mravlje, M. Ferrero, O. Parcollet, and I. A. Abrikosov, Phys. Rev. B **90**, 155120 (2014).

[24] L. V. Pourovskii, J. Mravlje, A. Georges, S. I. Simak, and I. A. Abrikosov, New J. Phys. **19**, 073022 (2017).

[25] J. Xu, P. Zhang, K. Haule, J. Minar, S. Wimmer, H. Ebert, and R. E. Cohen, Phys. Rev. Lett. **121**, 096601 (2018).

[26] P. Zhang, R. E. Cohen, and K. Haule, Nature **517**, 605 (2015); **536**, 112 (2016).

[27] O. Yu. Vekilova, L. V. Pourovskii, I. A. Abrikosov, and S. I. Simak, Phys. Rev. B **91**, 245116 (2015).

[28] L. V. Pourovskii, J. Phys.: Condens. Matter **31**, 373001 (2019).

[29] K. Shimizu, T. Kimura, S. Furomoto, K. Takeda, K. Kontani, Y. Onuki, and K. Amaya, Nature (London) **412**, 316 (2000).

[30] A. T. Holmes, D. Jaccard, G. Behr, Y. Inada, and Y. Onuki, J. Phys.: Condens. Matter **16**, S1121 (2004).

[31] J. Flouquet, in *Progress in Low Temperature Physics*, edited by W. P. Halperin (Elsevier, Amsterdam, 2005), p. 139.

[32] D. Jaccard, A. T. Holmes, G. Behr, Y. Inada, and Y. Onuki, Phys. Lett. A **299**, 282 (2002).

[33] D. Jaccard and A. T. Holmes, Physica B **359-361**, 333 (2005).

[34] P. Pedrazzini, D. Jaccard, G. Lapertot, J. Flouquet, Y. Inada, H. Kohara, and Y. Onuki, Physica B **378-380**, 165 (2006).

[35] K. Sengupta, P. Pedrazzini, and D. Jaccard, J. Phys: Conf. Ser. **200**, 012180 (2010).

[36] C. S. Yadav, G. Seyfarth, P. Pedrazzini, H. Wilhelm, R. Černý, and D. Jaccard, Phys. Rev. B **88**, 054110 (2013).

[37] T. Moriya, *Spin Fluctuations in Itinerant Electron Magnetism* (Springer, Berlin, 1985).

[38] I. I. Mazin, D. A. Papaconstantopoulos, and M. J. Mehl, Phys. Rev. B **65**, 100511(R) (2002).

[39] S. K. Bose, O. V. Dolgov, J. Kortus, O. Jepsen, and O. K. Andersen, Phys. Rev. B **67**, 214518 (2003).

[40] T. Jarlborg, Phys. Lett. A **300**, 518 (2002); Physica C **385**, 513 (2003).

[41] A. Dewaele, P. Loubeyre, F. Occelli, M. Mezouar, P. I. Dorogokupets, and M. Torrent, Phys. Rev. Lett. **97**, 215504 (2006).

[42] Dm. Korotin, A. V. Kozhevnikov, S. L. Skornyakov, I. Leonov, N. Binggeli, V. I. Anisimov, and G. Trimarchi, Eur. Phys. J. B **65**, 91 (2008).

[43] A. S. Belozerov and V. I. Anisimov, J. Phys.: Condens. Matter **26**, 375601 (2014).

[44] http://amulet-code.org.

[45] A. N. Rubtsov, V. V. Savkin, and A. I. Lichtenstein, Phys. Rev. B **72**, 035122 (2005); P. Werner, A. Comanac, L. de Medici, M. Troyer, and A. J. Millis, Phys. Rev. Lett. **97**, 076405 (2006).

[46] W. Metzner and D. Vollhardt, Phys. Rev. Lett. **62**, 324 (1989); A. Georges, G. Kotliar, W. Krauth, and M. J. Rozenberg, Rev. Mod. Phys. **68**, 13 (1996).

[47] T. Maier, M. Jarrell, T. Prushke, and M. H. Hettler, Rev. Mod. Phys. **77**, 1027 (2005).

[48] G. Rohringer, H. Hafermann, A. Toschi, A. A. Katanin, A. E. Antipov, M. I. Katsnelson, A. I. Lichtenstein, A. N. Rubtsov, and K. Held, Rev. Mod. Phys. **90**, 025003 (2018).

[49] A. A. Katanin, A. I. Poteryaev, A. V. Efremov, A. O. Shorikov, S. L. Skornyakov, M. A. Korotin, and V. I. Anisimov, Phys. Rev. B **81**, 045117 (2010).

[50] P. A. Igoshev, A. V. Efremov, A. I. Poteryaev, A. A. Katanin, and V. I. Anisimov, Phys. Rev. B **88**, 155120 (2013).

[51] A. S. Belozerov, A. A. Katanin, and V. I. Anisimov, Phys. Rev. B **96**, 075108 (2017).

[52] H. J. Vidberg and J. W. Serene, J. Low Temp. Phys. **29**, 179 (1977).

[53] A. V. Chubukov and D. L. Maslov, Phys. Rev. B **86**, 155136 (2012).

[54] The spin-spin correlation function for α-iron was calculated by DFT+DMFT method at $\beta = 40\,\mathrm{eV}^{-1}$ with interaction parameters $U = 4$ eV and $J = 0.9$ eV. Details of calculations are presented in Refs. [49–51].

[55] A. Toschi, R. Arita, P. Hansmann, G. Sangiovanni, and K. Held, Phys. Rev. B **86**, 064411 (2012).

[56] S. L. Skornyakov, A. A. Katanin, and V. I. Anisimov, Phys. Rev. Lett. **106**, 047007 (2011).

[57] K. Wilson, Rev. Mod. Phys. **47**, 773 (1975).

[58] V. I. Mel'nikov, Sov. Phys. JETP Lett. **35**, 511 (1982).

[59] A. M. Tsvelick and P. B. Wiegmann, Adv. Phys. **32**, 453 (1983).

[60] W. Kohn and J. M. Luttinger, Phys. Rev. Lett. **15**, 524 (1965).

[61] S. Raghu, S. A. Kivelson, and D. J. Scalapino, Phys. Rev. B **81**, 224505 (2010); W. Cho, R. Thomale, S. Raghu, and S. A. Kivelson, *ibid.* **88**, 064505 (2013).

[62] S. Raghu, A. Kapitulnik, and S. A. Kivelson, Phys. Rev. Lett. **105**, 136401 (2010); S. Raghu, S. B. Chung, and S. Lederer, J. Phys.: Conf. Series **449**, 012031 (2013).

[63] D. J. Scalapino, E. Loh, Jr., and J. E. Hirsch, Phys. Rev. B **34**, 8190(R) (1986); **35**, 6694 (1987).

[64] J. Otsuki, H. Hafermann, and A. I. Lichtenstein, Phys. Rev. B **90**, 235132 (2014).

[65] M. Kitatani, T. Schäfer, H. Aoki, and K. Held, Phys. Rev. B **99**, 041115(R) (2019).

[66] A. A. Katanin, A. Toschi, and K. Held, Phys. Rev. B **80**, 075104 (2009).

[67] N. Bulut, D. J. Scalapino, and S. R. White, Phys. Rev. B **47**, 6157(R) (1993).

[68] The eigenvalue $\lambda=1$ corresponds to the pairing instability. In view of our qualitative analysis of the second-order perturbation theory we find only the eigenfunctions, corresponding to the leading eigenvalue, and do not obtain corresponding pairing temperatures.

[69] T. Kuwabara and M. Ogata, Phys. Rev. Lett. **85**, 4586 (2000).

[70] S. V. Vonsovskii, M. I. Katsnelson, and A. V. Trefilov, Phys. Met. Metallogr. **76**, 247 (1993); J. Magn. Magn. Mat. **61**, 83 (1986).

[71] W. A. Basset and H. Wang, Science **238**, 780 (1987).